



Applicability of dragon fruit (*Hylocereus polyrhizus*) peels as low-cost biosorbent for adsorption of methylene blue from aqueous solution: kinetics, equilibrium and thermodynamics studies

Ali H. Jawad^{a,*}, Afaf Murtadha Kadhum^b, Y.S. Ngoh^c

^aFaculty of Applied Sciences, Universiti Teknologi MARA, 40450 Shah Alam, Selangor, Malaysia, Tel. +60355211721; emails: ahjm72@gmail.com, ali288@salam.uitm.edu.my

^bChemistry Department, College of Science, Al-Muthanna University, Iraq, Tel. +9647816827372; email: afafmurtadha@yahoo.com

^cSchool of Chemical Sciences, Universiti Sains Malaysia, 11800 Minden, Penang, Malaysia, Tel. +604 6534031; email: nyingshin@yahoo.com

Received 30 July 2017; Accepted 1 February 2018

ABSTRACT

This study evaluated the feasibility of utilizing agricultural waste dragon fruit (*Hylocereus undatus*) peels (DFP) as natural low-cost adsorbent to remove cationic dye methylene blue (MB) from aqueous solution. The physicochemical compositions of the DFP were characterized using CHNS-O analysis, X-ray diffraction, scanning electron microscopy, Fourier transform infrared spectroscopy and point of zero charge (pH_{pzc}) method. Batch mode adsorption studies were carried out by varying the operational parameters, namely adsorbent dosage (0.02–0.20 g), pH (3–10), initial MB concentration (50–400 mg/L) and contact time (0–120 min). The adsorption kinetic data showed that the process was best described by the pseudo-second-order kinetic model. The equilibrium data were discovered to better obeyed the Langmuir isotherm model than the Freundlich with maximum monolayer adsorption capacity, q_m , of the DFP towards MB was found to be as high as 192.31 mg/g. The thermodynamic adsorption parameters such as standard enthalpy (ΔH°), standard entropy (ΔS°) and standard free energy (ΔG°) advocated that the adsorption of MB by DFP was endothermic and spontaneous under the tested conditions. These findings clearly indicated the viability of DFP as an effective adsorbent for elimination of MB from aqueous solution.

Keywords: Adsorption; Agricultural waste; Dragon fruit peel; Low-cost adsorbent; Methylene blue

1. Introduction

The discharge of colored effluents from various dyes consuming industries is a major environmental issue due to its detrimental effects towards many living beings. The presence of dyes in water obstructs the accessibility of sunlight into the water, obstructs photosynthesis and eventually causes the disruption of aquatic life-cycle [1]. Dyes are also known to be toxic and carcinogenic which could cause detrimental health effects. Nonetheless, the usages of synthetic dyes in various industries have increased significantly over the years

due to its simple applicability and persistent dyeing effect. Thus, it is impossible to reverse the use of synthetic dyes, and therefore more feasible to come up with an efficient and cost-effective treatment method to eliminate dyes in colored effluents [2].

Methylene blue (MB), a cationic basic dye which forms face-to-face dimers, represents one of the most widely utilized synthetic dyes not only in the dyeing industries but also in the field of chemistry, biology and medical science [3]. Some of the health complications due to long-term exposure to MB include eye burns, breathing difficulties, nausea, allergy, vomiting, mental confusion, jaundice and even dysfunction of brain, liver and central nervous system [4]. Following this,

* Corresponding author.

many wastewater treatment methods including adsorption [5–9], electrochemical treatment [10], membrane filtration [11], Fenton chemical oxidation [12], photocatalysis [13–16] have been studied extensively for effective elimination of MB. Among these techniques, adsorption is preferred due to its effectiveness, simplicity, flexibility and ease of operation without generating hazardous secondary products [17,18]. There are many types of adsorbents utilized for the removal of MB with activated carbon as the most commonly used adsorbent to remove MB. However, activated carbon is deemed too costly and hard to be regenerated.

Agricultural waste peels have been considered as an ecological burden for the society. Anyhow, waste peels, as lignocellulosic biomass-rich materials, have stimulated new gateways for the production of renewable, low cost and sustainable adsorbents for water treatment applications. Fruit and vegetable peels consist of the highest percentage of wastes in most kitchen garbage bins. Furthermore, in fruit and vegetable industries, it is common that some waste is generated during processing (selecting, sorting and boiling processes) [19]. Processing of fruits and vegetables produces different types of waste including a solid waste of peel/skin. Plenty of the fruits and vegetables skins (peels) are discarded in the garbage. Fruits and vegetables wastes and by-products, which are formed in great amounts during industrial processing, represent a serious problem, as they exert an influence on environment and need to be managed and/or utilized [19].

Therefore, there have been demands for cost-effective adsorbents such as biomass wastes to make the adsorption process a viable wastewater treatment technology. Hence, recent years have seen many adsorption studies applying fruit peels such as orange peel [20,21], mango peel [8], pomelo peel [22], grapefruit peel [23], lemon peel [24], banana peel [21,25,26], jackfruit peel [27], durian peel [28], passion fruit peel [29,30] and dragon fruit foliage [31,32] for removing dyes from aqueous solution via adsorption process.

Dragon fruit, also known as pitaya, is a type of tropical fruits under the cactus family, *Cactaceae* and one of the commonly found dragon fruit species in Malaysia is the red dragon fruit (*Hylocereus polyrhizus*). The red dragon fruit typically weighs about 350 g and is best grown in dry, tropical or subtropical climate condition with one plant producing up to six cycles of fruits per year [33]. The average yield of dragon fruit in Malaysia is in the range of 16,000–27,000 kg/ha [34]. Known for its antioxidant and refreshing properties, the pulp of the red dragon fruit is usually consumed directly or processed into juice and recently has been promoted as natural food additives. Nonetheless, the red dragon fruit peel (DFP) is discarded as waste which possesses no commercial value. The DFP primarily contains triterpenoids, steroids, betanin, phyllocactin, hylocerenin, betacyanin and pectin which are abundant with functional groups such as hydroxyl, carboxyl and amine that can easily attract cationic compounds [35,36].

Thus, this present work investigates the application of DFP as a low cost adsorbent for MB removal from aqueous solution through batch mode adsorption studies. Batch mode adsorption experiments were performed by varying operational parameters such as adsorbent dosage, solution pH, initial MB concentration, contact time and temperature. The equilibrium adsorption data were fitted

to the Langmuir and Freundlich isotherm models while the attained kinetic data were fitted to pseudo-first-order (PFO) and pseudo-second-order (PSO) kinetic models. The thermodynamic profiles of the MB adsorption process by the DFP were also studied. The physicochemical properties of DFP before and after MB adsorption were probed in order to comprehend the adsorption behavior of MB onto DFP.

2. Materials and methods

2.1. Adsorbate (MB)

MB attained from R&M Chemicals, Malaysia, was applied as an adsorbate. All MB solutions were prepared and diluted with 18 M Ω cm ultrapure water. The used MB has a chemical formula of $C_{16}H_{18}Cl_3S \cdot xH_2O$ with molecular weight of 319.86 g/mol.

2.2. Preparation of DFP as adsorbent

The DFPs were obtained from a local fresh juice shop in Penang, Malaysia. DFP was first washed with boiled distilled water and then dried at 105°C in the oven for 24 h to remove the moisture contents. The dried DFP was subsequently ground and sieved to the size of 500–850 μ m. The ultimate elemental analysis of DFP was executed using a CHNS-O analyzer (PerkinElmer, Series II, 2400). X-ray diffraction (XRD) analysis was performed in order to determine the crystallinity or amorphous nature of DFP by XRD in reflection mode (Cu K α radiation) on a PANalytical, X'Pert Pro X-ray diffractometer. Scans were recorded with a scanning rate of 0.59°/s. The diffraction angle (2θ) was varied from 10° to 90°. The surface morphology of DFP before and after adsorption of MB was observed using a scanning electron microscope (SEM; FESEM CARL ZEISS, SUPKA 40 VP). The functional groups of DFP before and after MB were studied via Fourier transform infrared (FTIR) spectroscopy (PerkinElmer, Spectrum RX I) in transmission mode with a spectral range from 4,000 to 400 cm^{-1} with a resolution of 4 cm^{-1} . All samples were prepared with spectroscopic grade KBR which comprises ~80% (w/w) of the total sample and were evaluated in the form of finely ground powders. The pH at the point of zero charge (pH_{pzc}) was estimated by the solid addition method by using a pH meter (Metrohm, Model 827 pH Lab, Switzerland), as described by Lopez-Ramon et al. [37].

2.3. Batch mode adsorption experiments

The batch mode adsorption experiments of MB onto DFP surface were carried out in a series of 250 mL Erlenmeyer flasks containing 100 mL of MB solution. The flasks were capped and agitated in an isothermal water bath shaker (Mettler waterbath, model WNB7-45, Germany) at fixed shaking speed of 120 stroke/min and 303 K until equilibrium was achieved. Batch mode adsorption experiments were performed by varying several operational parameters such as adsorbent dosage (0.02–0.20 g), solution pH (3–10), initial MB concentration (50–400 mg/L) and contact time (0–120 min) to determine the optimum uptake conditions for MB adsorption. The pH of MB solution was adjusted by adding either 0.10 M HCl or NaOH. For the quantification of the adsorbed

MB, the supernatant of the DFP-MB mixture was collected with a 0.20 μm Nylon syringe filter and the concentrations of MB were monitored at different time interval using a HACH DR 2800 Direct Reading Spectrophotometer at the maximum wavelength (λ_{max}) of absorption at 661 nm. In the thermodynamic study, similar procedures were applied at 313 and 323 K, with the other parameters held constant. Blank tests were carried out to account for the color leached by the adsorbent and adsorbed by the glass containers, in which blank runs with only the adsorbents in 100 mL of ultrapure water and 100 mL of MB solution without any adsorbent were conducted concurrently at similar conditions. The adsorption capacity at equilibrium, q_e (mg/g) and the percentage of color removal, R_c (%) of MB were calculated using Eqs. (1) and (2):

$$q_e = \frac{C_o - C_e}{W} V \quad (1)$$

$$R_c (\%) = \frac{C_o - C_e}{C_o} \times 100 \quad (2)$$

where C_o is the initial MB concentration (mg/L); C_e is the MB concentration at equilibrium (mg/L); V is the volume of MB solution (L) and W is the dry mass of adsorbent DFP (g). Adsorption experiments were conducted in triplicate under identical conditions and the results are reported as an average value.

3. Results and discussion

3.1. Characterization of DFP

XRD pattern of the DFP sample is shown in Fig. 1. XRD pattern shows a broad hump indicating that DFP sample is amorphous in nature. However, a second hump at around 39.1° indicates that there exists a short-range crystallographic ordering in the DFP. No sharp peaks, indicative of any crystalline phase, can be observed from the XRD pattern.

The outcome of the ultimate elemental and EDX analyses of DFP is tabulated in Table 1. The result indicates

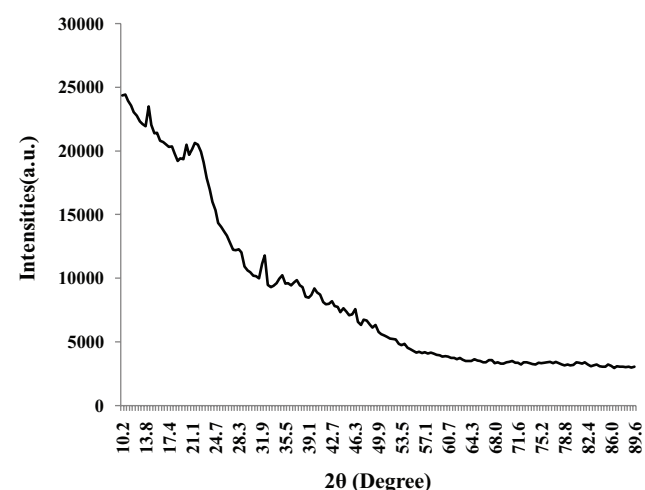


Fig. 1. XRD pattern of DFP.

that oxygen and carbon are the major constituents of DFP along with quantifiable amount of hydrogen and nitrogen. The pattern of adsorption onto biomass materials is highly associated to the availability of the active functional groups and bonds of the DFP surface. For the elucidation of these active sites, FTIR spectroscopy was performed upon the DFP before and after MB adsorption. Several IR bands appearing in the FTIR spectrum of DFP before adsorption (Fig. 2(a)) that signified various functional groups, in accordance with their respective wavenumber (cm^{-1}) position, are as reported by Ünler et al. [38]. The broad and intense band at $3,000\text{--}3,500\text{ cm}^{-1}$ are attributed by the --OH stretching vibrations of cellulose, pectin and lignin while the band at around $2,900\text{ cm}^{-1}$ corresponds to the --CH stretching vibrations of methyl group. The band at around $1,700\text{ cm}^{-1}$ indicates the C=O stretching of carboxylic acid or esters. The asymmetric and symmetric vibrations of --COO of the ionic carboxylic groups within DFP are represented by the band at around $1,650$ and $1,400\text{ cm}^{-1}$, respectively. The band at $1,380\text{ cm}^{-1}$ can be ascribed to the symmetric stretching of --COO of pectin. The IR bands between the $1,300$ and

Table 1
Ultimate analysis for dragon fruit peel (DFP)

| Ultimate analysis (wt%) | |
|-------------------------|--------------|
| C | 37.39 |
| H | 5.87 |
| N | 0.32 |
| S | Not detected |
| O (by difference) | 56.42 |
| EDX (wt%) | |
| C | 51.14 |
| O | 48.61 |
| Al | 0.16 |
| Ca | 0.09 |

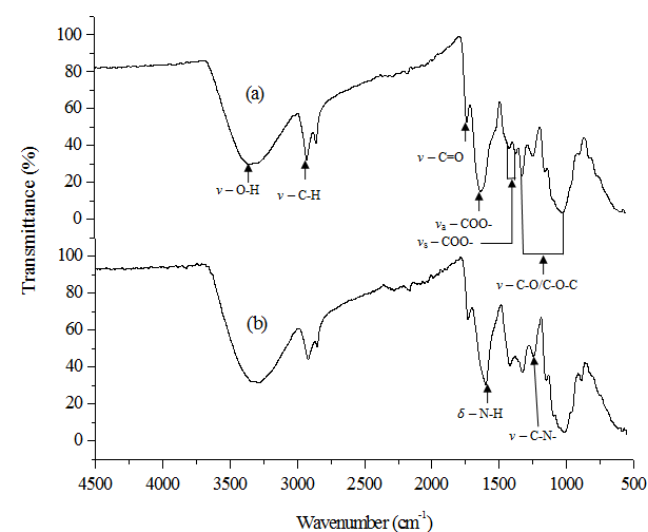


Fig. 2. FTIR spectra of DFP: (a) before MB adsorption and (b) after MB adsorption.

1,000 cm^{-1} region are assigned to the C–O and C–O–C stretching vibrations in carboxylic acids, alcohols, phenols or ester groups. Thus, the IR spectral of DFP before MB adsorption strongly shows that the external surface of DFP is rich in carboxylic and hydroxyl groups, which can be deprotonated to bind the positively charged MB. As depicted by the IR spectra of DFP after MB adsorption (Fig. 2(b)), some of the bands shifted and became more pronounced in which the attenuated bands at about 1,620 cm^{-1} (–N–H bending) and 1,240 cm^{-1} (C–N vibration) suggest the interaction of MB molecules with the functional groups of DFP. The reductions in the band intensities upon adsorption were also observed by Kallel et al. [39] for the adsorption of MB onto garlic straw. The pH_{pzc} of DFP was determined to find out the pH at which the electrical charge of the surface of DFP was zero. Fig. 3 shows that the pH_{pzc} of DFP was at pH 4.3 which reflected the acidity of DFP, in agreement with the aforementioned IR results (Fig. 1) that carboxylic acids are present in abundance within DFP. Adsorption of anions is favored at solution pH below the pH_{pzc} value as the surface of DFP is positively charged due to protonation whereas at solution pH above the pH_{pzc} value, the surface of DFP becomes negatively charged and thus, adsorption of cations is preferred. In this regard, it is predicted that the adsorption of the cationic MB by DFP will be appropriate at solution pHs above 4.3 because of electrostatic interactions. The surface morphology of DFP before and after MB adsorption was observed based on the SEM images presented in Fig. 4. According to Fig. 4(a), the DFP before MB adsorption possesses heterogeneous, uneven, wavy and irregular surface which offers high possibility for MB molecules to be adsorbed. Thus, the SEM image of DFP after MB adsorption in Fig. 4(b) reveals more compact and less heterogeneous surface features due to the loading of MB molecules on the DFP surface.

3.2. Batch mode adsorption of MB

3.2.1. Effect of adsorbent dosage

The effect of the adsorbent dosage on the removal of MB by DFP was studied using varying amount of DFP, ranging from 0.02 to 0.20 g at fixed MB volume of 100 mL and initial

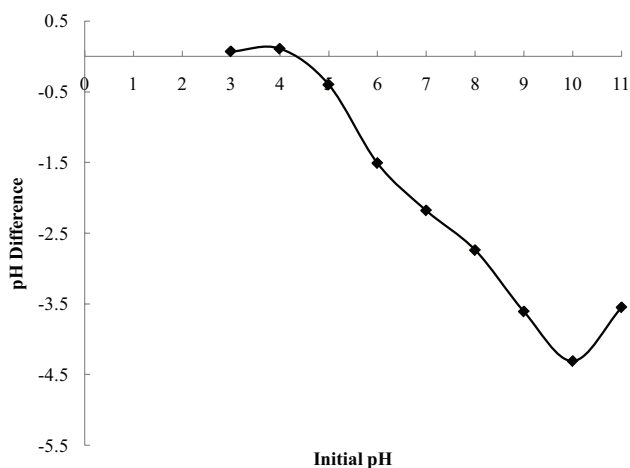


Fig. 3. pH_{pzc} of DFP suspensions.

dye solution, C_0 , of 100 mg/L. During this experiment, other operational parameters were held constant at 303 K, shaking speed of 120 stroke/min, contact time of 120 min and an unadjusted pH value of 5.6 for the initial MB solution. The results are depicted in Fig. 5, whereby it is learnt that the removal MB increased proportionally with the DFP dosage until 0.06 g and further addition rendered no significant impact on the MB removal percentage. The increase in the MB removal with the increasing mass of DFP was attributed to the greater number of adsorption sites on the adsorbent surface which allowed more bindings of MB molecules with DFP [40,41]. However, further addition of DFP dosage beyond 0.06 g did not see any improvement in the adsorption percentage of MB. This observation could be caused by the aggregations of DFP particles at higher dosages which led to decrease in the effective surface area of DFP for MB uptake. Therefore, 0.06 g of DFP was selected for the following experiments.

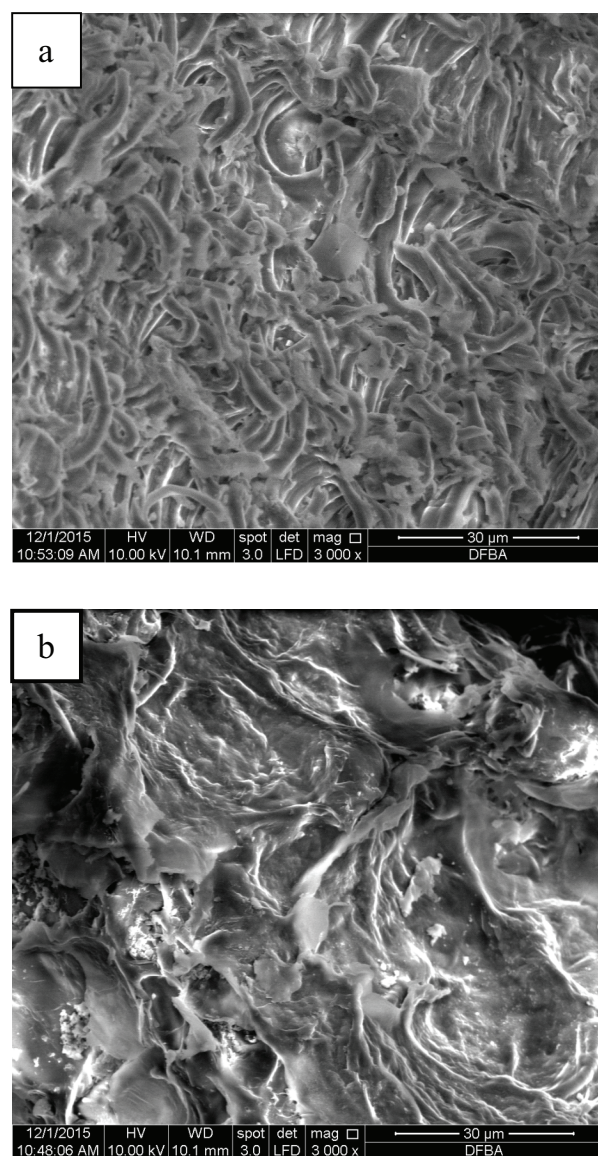


Fig. 4. SEM micrograph of DFP particle (3,000 magnification): (a) before MB adsorption and (b) after MB adsorption.

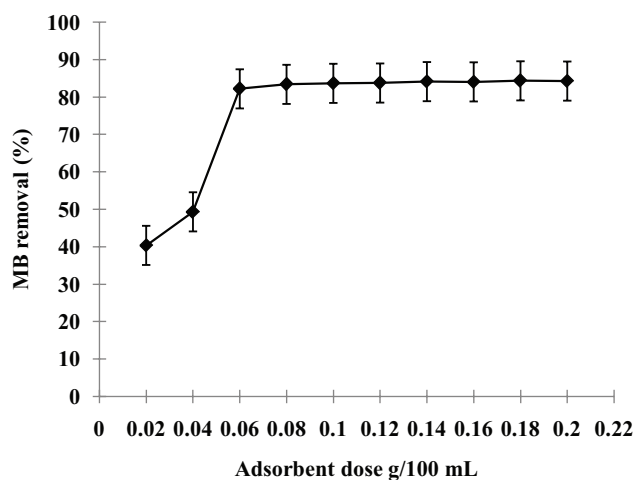


Fig. 5. Effect of DFP dosage on the removal of MB (%) at $[MB]_0 = 100$ mg/L, $V = 100$ mL, $pH = 5.60$ (unadjusted), $T = 303$ K, shaking speed = 120 stroke/min and contact time = 180 min.

3.2.2. Effect of pH

The pH value of the solution, which influences the surface charge of the adsorbent and the speciation magnitude of dye, plays a vital role in governing the adsorption process. Fig. 6 shows the effect of pH on the adsorption of MB onto DFP. As observed, the adsorption of MB onto DFP increased gradually with the increasing solution pH up to pH 5.0 after which further increase in pH values exhibited no significant changes. Lower value of adsorption capacity at acidic pH may be either due to excess concentration of H^+ ions competing with the MB dye cations for adsorption sites. Moreover, at solution $pH < pH_{pzc} = 4.3$, the surface of DFP was essentially positively charged and thus, repulsion between the MB cations and the DFP may have occurred and decreased the MB adsorption capacity. On the other hand, as the pH of the process increased, the surface of DFP was likely to adopt negative surface charges and became increasingly favorable for MB adsorption due to electrostatic forces of attraction. The observation that the adsorption of MB remained almost constant from pH 5.0 onwards may be due to the complete deprotonation of the active group, that is, $COOH \rightarrow COO^-$ of DFP surface when the solution pH surpassed 5.0 [42]. Thus, the optimum pH for the removal of MB by DFP was at pH 5.0 and above. Since the unadjusted pH of the initial MB solution (5.6) lies within the optimal pH range and in order to lessen chemical and time consumptions, further experiments on the adsorption of MB by DFP were conducted at pH 5.6.

3.2.3. Effect of initial dye concentration and contact time

The effect of initial MB concentration and contact time on MB adsorption onto DFP is depicted in Fig. 7. As seen, the MB adsorption profiles at all concentration shows that the adsorption process at the initial stage was fast with respect to the contact time and gradually became slower as equilibrium state was approached. At the initial stage of the adsorption process, there were more vacant active surface sites of DFP which were available for the uptake of MB molecules and as the time lapsed, the availability of the sites became limited

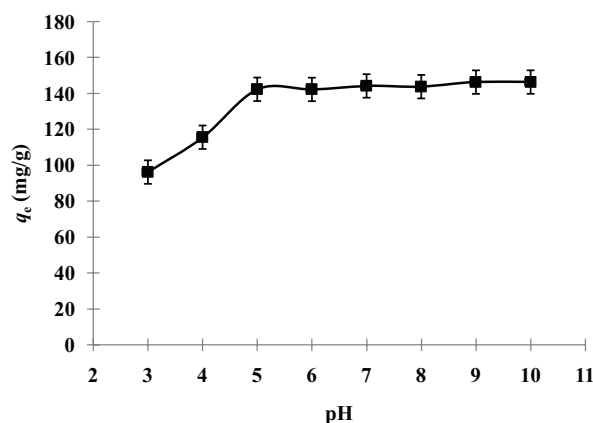


Fig. 6. Effect of pH on the adsorption capacity of MB by DFP at $[MB]_0 = 100$ mg/L, $V = 100$ mL, $T = 303$ K, shaking speed = 120 stroke/min, contact time = 180 min and DFP dosage = 0.06 g.

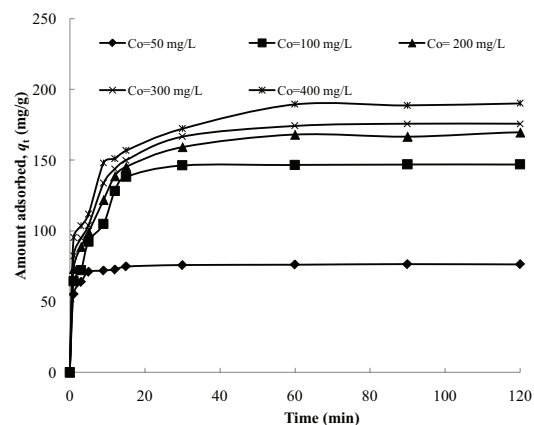


Fig. 7. Effects of initial dye concentration and contact time on the adsorption capacity of MB by DFP ($V = 200$ mL, $T = 303$ K, $pH = 5.6$, shaking speed = 120 stroke/min and DFP dosage = 0.12 g).

which led to the slowing down of the process. The increase in the initial concentration of MB, however, increased the adsorption capacity of DFP. The amount of MB adsorbed by DFP at equilibrium increased significantly from 75.8 to 190.3 mg/g as the initial concentration of MB was increased from 50 to 400 mg/L. This effect can be ascribed to the enhanced driving force of the mass transport of MB molecules towards the active pores within the inner depth of DFP at higher initial dye concentration. At low initial MB concentration, even though the driving force was slower, the uptake of the limited amount of the dye by DFP led to faster establishment of the equilibrium state. However, at higher concentration of MB, the attainment of equilibrium state required longer time to achieve since higher driving force allowed the MB molecules to penetrate deeper into the porous interior of the adsorbent [28]. This explanation corroborates with the outcome of this experiment, whereby 50 mg/L of MB took 15 min to reach the adsorption equilibrium state while MB with concentration of 400 mg/L required 90 min. Hence, it is shown that initial dye concentration plays an important role in the adsorption capacity of MB by DFP.

3.3. Adsorption isotherm studies

The adsorption equilibrium data of MB onto DFP were assessed using the two commonly used isotherm models to describe the interaction between the adsorbent and the adsorbate with the quality of the fit evaluated using the coefficient of determination, R^2 values. The Langmuir isotherm model assumes that the adsorption is localized on a monolayer and all adsorption sites at the adsorbent are structurally homogeneous, with no interaction between molecules adsorbed on adjacent sites [43]. The adsorbent possesses the finite adsorption capacity in which no further adsorption can occur once a molecule occupied a site and reached an equilibrium saturation point [44]. The linear mathematical expression of Langmuir isotherm is represented by Eq. (3):

$$\frac{C_e}{q_e} = \frac{1}{q_m K_L} + \frac{1}{q_m} C_e \quad (3)$$

where C_e is the equilibrium concentration (mg/L) and q_e is the amount of adsorbed species per specified amount of adsorbent (mg/g) while K_L (L/mg) and q_m (mg/g) are the Langmuir constants associated to the adsorption affinity and capacity, respectively. Thus, a plot of C_e/q_e vs. C_e should yield a straight line with a slope ($1/q_m$) and intercept ($1/q_m K_L$) as shown in Fig. 8(a). On the contrary, the Freundlich adsorption isotherm is based on the assumption that the adsorption occurs on heterogeneous surfaces of non-identical sites with different energy of adsorption. This empirical isotherm model is often employed to describe multilayer adsorption with interaction between the adsorbed molecules and is not limited to monolayer formation of adsorbate molecules on the adsorbent [45]. The well-known linear mathematical form of Freundlich isotherm is shown by Eq. (4):

$$\ln q_e = \ln K_F + \frac{1}{n} \ln C_e \quad (4)$$

where K_F [$\text{mg/g (L/mg)}^{1/n}$] and $1/n$ are the Freundlich isotherm constants related to the adsorption capacity and intensity, respectively. The K_F and n values can be derived from the intercept and slope of the $\ln q_e$ vs. $\ln C_e$ plot given in Fig. 8(b). The adsorption parameters for both the isotherm models are listed in Table 2. The Langmuir isotherm model showed better fit for the MB adsorption equilibrium data, as evidenced by the greater R^2 value as compared with that of the Freundlich model. Based on the Freundlich isotherm model, the slope, $1/n$ ranging between 0 and 1, is a measure of surface heterogeneity, whereby the surface is more heterogeneous as the $1/n$ value approaches zero. A value of $1/n < 1$ indicates a normal Langmuir isotherm while $1/n > 1$ is reflective of cooperative adsorption [46]. Moreover, the value of exponent $n > 1$ is an implication of a favorable adsorption process. In this case, the obtained $1/n$ value for DFP is below unity, indicating that the favorable MB adsorption process and reconfirmed a normal Langmuir isotherm characteristic. These results affirmed that the surface binding sites of DFP are homogeneous in nature whereby each MB is attached with similar adsorption energy. The results show that the formation of a surface monolayer of MB molecules for DFP, in which the monolayer adsorption

capacity, q_m for DFP towards MB was compared against that of the other types of fruit peels in Table 3. As listed in Table 3, DFP exhibits higher MB adsorption capacity when compared with some of the untreated fruit peels. This proves the viability of DFP as one of the most superior adsorbents for removal of MB from aqueous solution.

3.4. Adsorption kinetic studies

The adsorption kinetic of MB onto DFP data was analyzed using the PFO and PSO model to determine the adsorption rate and to explain the adsorbate–adsorbent interactions that occurred. The conformity between the experimental data and the model predicted values was presented by the coefficient of determination, R^2 values. The PFO is constructed based on the prediction that the change of adsorbate uptake rate

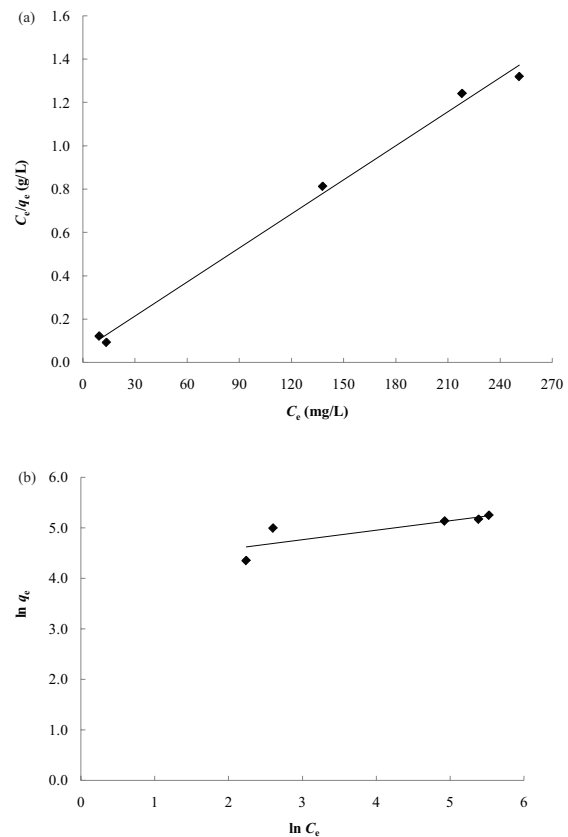


Fig. 8. Isotherm models for the adsorption of MB onto DFP at 303 K: (a) Langmuir and (b) Freundlich.

Table 2
Isotherm parameters for adsorption of MB onto DFP at 303 K

| Langmuir isotherm | | |
|---------------------------------|--------------|-------|
| q_m (mg/g) | K_L (L/mg) | R^2 |
| 192.31 | 0.091 | 0.995 |
| Freundlich isotherm | | |
| K_F [(mg/g) (L/mg) $^{1/n}$] | $1/n$ | R^2 |
| 66.57 | 0.189 | 0.682 |

Table 3
Comparison of adsorption capacities for MB by different untreated fruit peels adsorbents

| Fruit peels adsorbents | Adsorbent dosage (g) | Adsorption capacity, q_m (mg/g) | References |
|---------------------------|----------------------|-----------------------------------|------------|
| Dragon fruit peel (DFP) | 0.06 g/100 mL | 192.31 | This work |
| Jackfruit peel | 0.60 g/200 mL | 285.71 | [27] |
| Orange peel | 0.10 g/100 mL | 218 | [20] |
| Pomelo peel | 0.40 g/100 mL | 133 | [22] |
| Banana peel | 0.10 g/100 mL | 111.11 | [26] |
| Yellow passion fruit peel | 1 g/100 mL | 44.7 | [30] |
| Banana peel | 0.10 g/100 mL | 20.80 | [21] |
| Banana peel | 1 g/1,000 mL | 18.65 | [25] |
| Orange peel | 0.10 g/100 mL | 18.60 | [21] |

with time is proportional to the difference in concentration at equilibrium and the amount of adsorbed adsorbate with time [47] and is expressed as Eq. (5):

$$\ln(q_e - q_t) = \ln(q_e) - k_1 t \tag{5}$$

where q_e (mg/g) and q_t (mg/g) are the amount of adsorbate adsorbed onto adsorbent at equilibrium and time t , respectively, while k_1 is the PFO rate constant. The k_1 values can be determined from the slope of the plot of $\ln(q_e - q_t)$ vs. t shown in Fig. 9(a). Meanwhile, the PSO is based on the assumption that the rate-limiting step of the adsorption process may be chemisorption involving sharing or exchange of electrons between adsorbent and adsorbate [48]. The linear form of the PSO model is described by Eq. (6):

$$\frac{t}{q_t} = \frac{1}{k_2 q_e^2} + \frac{t}{q_e} \tag{6}$$

where k_2 (g/min mg) is the PSO rate constant. The k_2 and theoretical $q_{e,cal}$ values can be calculated from the intercept and slope of the t/q_t vs. t plot depicted in Fig. 9(b). The kinetic data for the adsorption of MB onto DFP were calculated from the related plots and are tabulated in Table 4. The presented data shows that the MB adsorption kinetic data were better fitted by the PSO model with R^2 values of ≥ 0.965 for all tested concentrations. This result infers that the rate of MB adsorption onto DFP seemed to be governed by chemical process that involved sharing of electrons or by covalent forces through exchanging of electrons between adsorbent and adsorbate.

3.5. Adsorption thermodynamics studies

The thermodynamic parameters of adsorption of MB onto DFP were derived from the experimental data obtained at 303, 313 and 323 K to deduce the nature and thermodynamic feasibility of the adsorption process. The standard free energy change (ΔG°), enthalpy change (ΔH°) and entropy change (ΔS°) related to the adsorption processes are calculated using Eqs. (7)–(9):

$$k_d = \frac{q_e}{C_e} \tag{7}$$

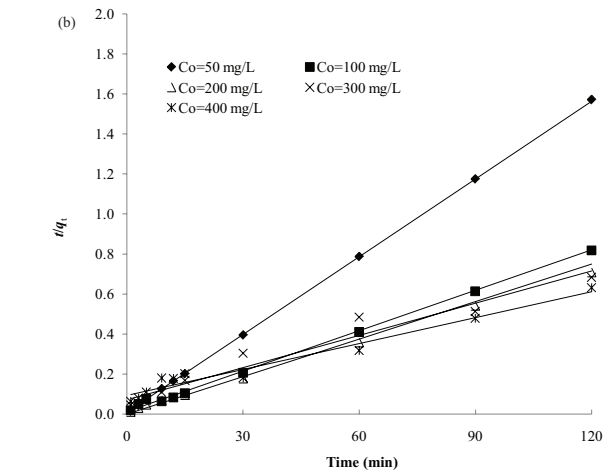
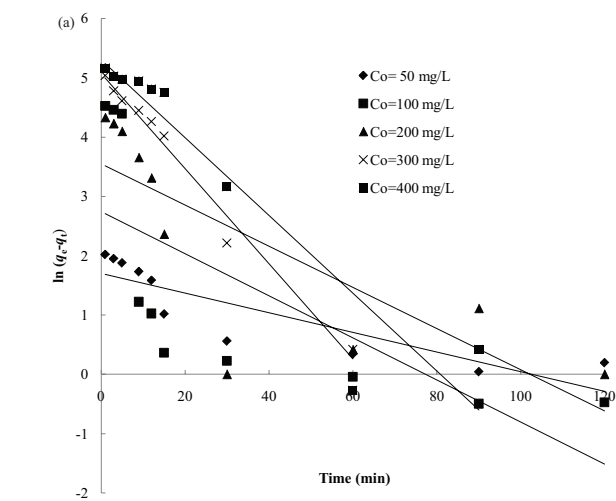


Fig. 9. Kinetic profiles for the adsorption of MB onto DFP at 303 K: (a) pseudo-first-order and (b) pseudo-second-order.

$$\Delta G^\circ = -RT \ln k_d \tag{8}$$

$$\ln k_d = \frac{\Delta S^\circ}{R} - \frac{\Delta H^\circ}{RT} \tag{9}$$

Table 4
Comparison of the pseudo-first-order (PFO) and pseudo-second-order (PSO) models for the adsorption of MB onto DFP at 303 K

| | Concentration (mg/L) | | | | |
|----------------------------|----------------------|--------|--------|--------|--------|
| | 50 | 100 | 200 | 300 | 400 |
| $q_{e,exp}$ | 77.63 | 147.62 | 169.71 | 175.80 | 190.26 |
| PFO | | | | | |
| $q_{e,cal}$ | 5.50 | 15.54 | 34.78 | 160.05 | 201.02 |
| k_1 (min ⁻¹) | 0.017 | 0.036 | 0.035 | 0.080 | 0.066 |
| R^2 | 0.766 | 0.794 | 0.637 | 0.983 | 0.814 |
| PSO | | | | | |
| $q_{e,cal}$ | 77.52 | 149.25 | 172.41 | 188.68 | 232.56 |
| k_2 | 0.018 | 0.004 | 0.003 | 0.0007 | 0.0002 |
| R^2 | 1.000 | 1.000 | 1.000 | 0.998 | 0.965 |

where k_d is the distribution coefficient, q_e is the concentration of MB adsorbed onto DFP at equilibrium (mg/L), C_e is the equilibrium of MB in the liquid phase (mg/L), R is the universal gas constant (8.314 J/mol K) and T is the absolute temperature (K). The values of ΔH° and ΔS° were calculated from the slope and intercept of Van't Hoff plot ($\ln k_d$ vs. $1/T$) given in Fig. 10 and the values of the parameters are listed in Table 5. As the adsorption temperature increased, the values of k_d increased as well, indicating that the MB adsorption capacity of DFP increased with the rise of temperature and this suggested that the adsorption process was an endothermic in nature. The negative ΔG° values advocated that the adsorption process was spontaneous and more favorable at low temperature. The positive value of ΔH° (5.40 kJ/mol) confirmed the endothermic nature of the adsorption process and the positive ΔS° (37.6 J/mol K) value revealed the increase in the randomness at solid–solution interface. There is unequal release of energy during the adsorption process and the magnitude of ΔH° value offers information about the forces that governed the adsorption process. The energy (ΔH°) related to physical forces: van der Waals (4–10 kJ/mol), hydrophobic interaction (5 kJ/mol), hydrogen bonding (2–40 kJ/mol), coordination exchange (40 kJ/mol), dipole bond forces (2–29 kJ/mol) and electrostatic interaction (20–80 kJ/mol) while for chemical forces (>60 kJ/mol) [49]. In this work, the ΔH° value was found to be 5.40 kJ/mol, confirming that physical forces were involved in the adsorption of MB onto DFP.

4. Conclusion

The biomass waste DFP exhibited great potential as low-cost adsorbent for effective removal of MB from aqueous solution. Physicochemical characterizations revealed that the carboxyl and hydroxyl groups of DFP play important role in the adsorption of MB. The optimum DFP dosage was 0.06 g and superior MB adsorption capacity was obtained in solution pH 5 onwards. The adsorption increased with increasing MB concentration. The adsorption equilibrium data obeyed

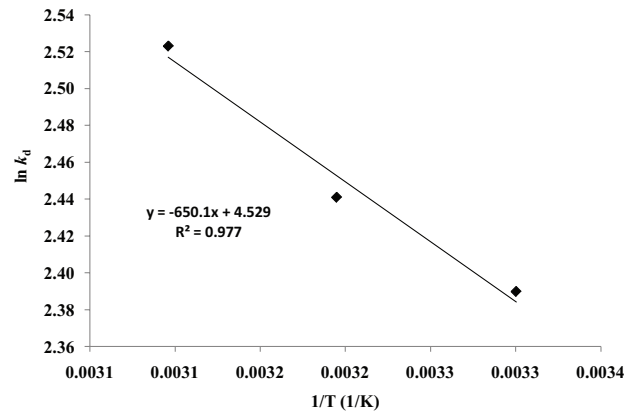


Fig. 10. Plot of $\ln k_d$ vs. $1/T$ for calculation of thermodynamic parameters for the adsorption of MB onto DFP.

Table 5
Thermodynamic parameters values for the adsorption of MB onto DFP

| Temperature (K) | Thermodynamics parameters | | | |
|-----------------|---------------------------|------------------------------|------------------------------|-------------------------------|
| | k_d | ΔG° (kJ/mol) | ΔH° (kJ/mol) | ΔS° (J/mol K) |
| 303 | 10.91 | -6.006 | | |
| 313 | 11.48 | -6.382 | 5.40 | 37.6 |
| 323 | 12.47 | -6.759 | | |

the Langmuir isotherm model and the monolayer adsorption capacity, q_m was found to be 192.31 mg/g. Meanwhile, the PSO model was determined to be better fit for the kinetic data as compared with the PFO model. The thermodynamic parameters values showed that the MB adsorption by DFP was a spontaneous and an endothermic in nature.

References

- [1] Z. Al-Qodah, W.K. Lafi, Z. Al-Anber, M. Al-Shannag, A. Harahsheh, Adsorption of methylene blue by acid and heat treated diatomaceous silica, *Desalination*, 217 (2007) 212–224.
- [2] N.S.A. Mubarak, A.H. Jawad, W.I. Nawawi, Equilibrium, kinetic and thermodynamic studies of Reactive Red 120 dye adsorption by chitosan beads from aqueous solution, *Energy Ecol. Environ.*, 2 (2017) 85–93.
- [3] A.H. Jawad, A.F.M. Alkarkhi, N.S.A. Mubarak, Photocatalytic decolorization of methylene blue by an immobilized TiO₂ film under visible light irradiation: optimization using response surface methodology (RSM), *Desal. Wat. Treat.*, 56 (2015) 161–172.
- [4] A.H. Jawad, N.S.A. Mubarak, M.A.M. Ishak, K. Ismail, W.I. Nawawi, Kinetics of photocatalytic decolorization of cationic dye using porous TiO₂ film, *J. Taibah Univ. Sci.*, 10 (2016) 352–362.
- [5] R.A. Rashid, A.H. Jawad, M.A.M. Ishak, N.N. Kasim, KOH-activated carbon developed from biomass waste: adsorption equilibrium, kinetic and thermodynamic studies for methylene blue uptake, *Desal. Wat. Treat.*, 57 (2016) 27226–27236.
- [6] A.H. Jawad, R.A. Rashid, R.M.A. Mahmud, M.A.M. Ishak, N.N. Kasim, K. Ismail, Adsorption of methylene blue onto coconut (*Cocos nucifera*) leaf: optimization, isotherm and kinetic studies, *Desal. Wat. Treat.*, 57 (2016) 8839–8853.

- [7] A.H. Jawad, R.A. Rashid, M.A.M. Ishak, L.D. Wilson, Adsorption of methylene blue onto activated carbon developed from biomass waste by H_2SO_4 activation: kinetic, equilibrium and thermodynamic studies, *Desal. Wat. Treat.*, 57 (2016) 25194–25206.
- [8] A.H. Jawad, N.F.H. Mamat, M.F. Abdullah, K. Ismail, Adsorption of methylene blue onto acid-treated mango peels: kinetic, equilibrium and thermodynamic study, *Desal. Wat. Treat.*, 59 (2017) 210–219.
- [9] A.H. Jawad, M.A.M. Ishak, A.M. Farhan, K. Ismail, Response surface methodology approach for optimization of color removal and COD reduction of methylene blue using microwave-induced NaOH activated carbon from biomass waste, *Desal. Wat. Treat.*, 62 (2017) 208–220.
- [10] M.S. Indu, A.K. Gupta, C. Sahoo, Electrochemical oxidation of methylene blue using lead acid battery anode, *APCBEE Procedia*, 9 (2014) 70–74.
- [11] Q. Li, Y. Li, X. Ma, Q. Du, K. Sui, D. Wang, C. Wang, H. Li, Y. Xia, Filtration and adsorption properties of porous calcium alginate membrane for methylene blue removal from water, *Chem. Eng. J.*, 316 (2017) 623–630.
- [12] L. Shen, P. Yan, X. Guo, H. Wei, X. Zheng, Three-dimensional electro-Fenton degradation of methylene blue based on the composite particle electrodes of carbon nanotubes and nano- Fe_3O_4 , *Arabian J. Sci. Eng.*, 39 (2014) 6659–6664.
- [13] W.I.N.W. Ismail, S.K. Ain, R. Zaharudin, A.H. Jawad, M.A.M. Ishak, K. Ismail, S. Sahid, New TiO_2 /DSAT immobilization system for photodegradation of anionic and cationic dyes, *Int. J. Photoenergy*, 2015 (2015) 1–6.
- [14] M.A. Nawawi, Y.S. Ngoh, S.M. Zain, Photoetching of immobilized TiO_2 -ENR₃₀-PVC composite for improved photocatalytic activity, *Int. J. Photoenergy*, 2012 (2012) 1–12.
- [15] Y.S. Ngoh, M.A. Nawawi, Fabrication and properties of an immobilized P25/ TiO_2 -montmorillonite bilayer system for the synergistic photocatalytic-adsorption removal of methylene blue, *Mater. Res. Bull.*, 76 (2016) 8–21.
- [16] Y.S. Ngoh, M.A. Nawawi, Role of bentonite adsorbent sub-layer in the photocatalytic-adsorptive removal of methylene blue by the immobilized TiO_2 /bentonite system, *Int. J. Environ. Sci. Technol.*, 13 (2016) 907–926.
- [17] A.H. Jawad, M.A. Islam, B.H. Hameed, Cross-linked chitosan thin film coated onto glass plate as an effective adsorbent for adsorption of reactive orange 16, *Int. J. Biol. Macromol.*, 95 (2017) 743–749.
- [18] Z. Al-Qodah, Adsorption of methylene blue with diatomite, *J. Eng. Technol.*, 17 (1998) 128–137.
- [19] A. Bhatnagar, M. Sillanpaa, A. Witek-Krowiak, Agricultural waste peels as versatile biomass for water purification – a review, *Chem. Eng. J.*, 270 (2015) 244–271.
- [20] M. Boumediene, H. Benaïssa, B. George, S. Molina, A. Merlin, Characterization of two cellulosic waste materials (orange and almond peels) and their use for the removal of methylene blue from aqueous solutions, *Maderas. Ciencia y Tecnologia*, 17 (2015) 69–84.
- [21] G. Annadurai, R.-S. Juang, D.-J. Lee, Use of cellulose-based wastes for adsorption of dyes from aqueous solutions, *J. Hazard Mater.*, 92 (2002) 263–274.
- [22] S.X. Hou, Adsorption properties of pomelo peels against methylene blue dye wastewater, *Adv. Mater. Res.*, 634–638 (2013) 178–181.
- [23] A. Saeed, M. Sharif, M. Iqbal, Application potential of grapefruit peel as dye sorbent: kinetics, equilibrium and mechanism of crystal violet adsorption, *J. Hazard Mater.*, 179 (2010) 564–572.
- [24] A. Bhatnagar, E. Kumar, A.K. Minocha, B.-H. Jeon, H. Song, Y.-C. Seo, Removal of anionic dyes from water using *Citrus limonum* (Lemon) peel: equilibrium studies and kinetic modeling, *Sep. Sci. Technol.*, 44 (2009) 316–334.
- [25] K. Amela, M.A. Hassen, D. Kerroum, Isotherm and kinetic study of biosorption of cationic dye onto banana peel, *Energy Procedia*, 19 (2012) 286–295.
- [26] F. Moubarak, R. Atmani, I. Maghri, M. Elkouali, M. Talbi, M. Latifa, Elimination of methylene blue dye with natural adsorbent “banana peels powder”, *Global J. Sci. Front. Res. B Chem.*, 14 (2014) 39–44.
- [27] B.H. Hameed, Removal of cationic dye from aqueous solution using jackfruit peel as non-conventional low-cost adsorbent, *J. Hazard Mater.*, 162 (2009) 344–350.
- [28] B.H. Hameed, H. Hakimi, Utilization of durian (*Durio zibethinus* Murray) peel as low cost sorbent for the removal of acid dye from aqueous solutions, *Biochem. Eng. J.*, 39 (2008) 338–343.
- [29] F.A. Pavan, A.C. Mazzocato, Y. Gushikern, Removal of methylene blue dye from aqueous solutions by adsorption using yellow passion fruit peel as adsorbent, *Bioresour. Technol.*, 99 (2008) 3162–3165.
- [30] F.A. Pavan, E.C. Lima, S.L.P. Dias, A.C. Mazzocato, Methylene blue biosorption from aqueous solutions by yellow passion fruit waste, *J. Hazard. Mater.*, 150 (2008) 703–712.
- [31] Z.Z. Abidin, Z. Haddadian, M.A. Shavandi, M.H.S. Ismail, F.R. Ahmadun, Methylene blue removal from aqueous solution by *Hylocereus undatus* (dragon fruit) foliage, *Appl. Mech. Mater.*, 625 (2014) 864–869.
- [32] Z. Haddadian, M.A. Shavandi, Z.Z. Abidin, M.H.S. Ismail, A. Fakhrol-Razi, Methyl orange removal from aqueous solutions using dragon fruit (*Hylocereus undatus*) foliage, *Chem. Sci. Trans.*, 2 (2013) 900–910.
- [33] K.M. Herbach, F.C. Stintzinga, R. Carlea, Identification of heat-induced degradation products from purified betanin, phyllocactin and hydrocerein by high-performance liquid chromatography/electrospray ionization mass spectrometry, *Rapid Commun. Mass Spectrom.* 19 (2005) 2603–2616.
- [34] Y. Mizrahi, A. Nerd, Climbing and Columnar Cacti: New Arid Land Fruit Crops, J. Janick, J.E. Simm, Eds., Perspective on New Crops and New Uses, American Society of Horticultural Science Press, Alexandria, Virginia, pp. 358–366.
- [35] W.S. Choo, W.K. Yong, Antioxidant properties of two species of *Hylocereus* fruits, *Adv. Appl. Sci. Res.*, 2 (2011) 418–425.
- [36] H. Luo, Y. Cai, Z. Peng, T. Liu, S. Yang, Chemical composition and in vitro evaluation of the cytotoxic and antioxidant activities of supercritical carbon dioxide extracts of pitaya (dragon fruit) peel, *Chem. Cent. J.*, 8 (2014) 1–7.
- [37] M.V. Lopez-Ramon, F. Stoeckli, C. Moreno-Castilla, F. Carrasco-Marin, On the characterization of acidic and basic surface sites on carbons by various techniques, *Carbon*, 27 (1999) 1215–1221.
- [38] O. Üner, Ü. Geggel, Y. Bayrak, Preparation and characterization of mesoporous activated carbons from waste watermelon rind by using the chemical activation method with zinc chloride, *Arabian J. Chem.* (2015). doi: <http://dx.doi.org/10.1016/j.arabj.2015.12.004>.
- [39] F. Kallel, F. Chaari, F. Bouaziz, F. Beltaieb, R. Ghorbel, S.E. Chaabouni, Sorption and desorption characteristics for the removal of a toxic dye, methylene blue from aqueous solution by a low cost agricultural by-product, *J. Mol. Liq.*, 219 (2016) 279–288.
- [40] A.H. Jawad, S. Sabar, M.A.M. Ishak, L.D. Wilson, S.S.A. Norrahma, M.K. Talari, A.M. Farhan, Microwave-assisted preparation of mesoporous-activated carbon from coconut (*Cocos nucifera*) leaf by H_3PO_4 activation for methylene blue adsorption, *Chem. Eng. Commun.*, 204 (2017) 1143–1156.
- [41] A.H. Jawad, R.A. Rashid, K. Ismail, S. Sabar, High surface area mesoporous activated carbon developed from coconut leaf by chemical activation with H_3PO_4 for adsorption of methylene blue, *Desal. Wat. Treat.*, 74 (2017) 326–335.
- [42] C. Deng, J. Liu, W. Zhou, Y.K. Zhang, K.F. Du, Z.M. Zhao, Fabrication of spherical cellulose/carbon tubes hybrid adsorbent anchored with welan gum polysaccharide and its potential in adsorbing methylene blue, *Chem. Eng. J.*, 200–202 (2012) 452–458.
- [43] I. Langmuir, The adsorption of gases on plane surfaces of glass, mica and platinum, *J. Am. Chem. Soc.*, 40 (1918) 1361–1403.
- [44] F. Gimbert, N. Morin-Crini, F. Renault, P.-M. Badot, G. Crini, Adsorption isotherm models for dye removal by cationized starch-based materials in a single component system: error analysis, *J. Hazard. Mater.*, 157 (2008) 34–46.

- [45] H.M.F. Freundlich, Over the adsorption in solution, *J. Phys. Chem.*, 57 (1906) 385–470.
- [46] B.H. Hameed, A.T.M. Din, A.L. Ahmad, Adsorption of methylene blue onto bamboo-based activated carbon: kinetics and equilibrium studies, *J. Hazard. Mater.*, 141 (2007) 819–825.
- [47] S. Lagergren, About the theory of so called adsorption of soluble substances, *K. Sven. Vetensk.akad. Handl.*, 24 (1898) 1–39.
- [48] Y.S. Ho, G. McKay, Pseudo-second-order model sorption processes, *Process Biochem.*, 34 (1999) 451–465.
- [49] F.M. Machado, C.P. Bergmann, E.C. Lima, B. Royer, F.E. de Souza, I.M. Jauris, T. Calvete, S.B. Fagan, Adsorption of Reactive Blue 4 dye from water solutions by carbon nanotubes: experiment and theory, *Phys. Chem. Chem. Phys.*, 14 (2012) 11139–11153.